Basrah Journal for Engineering Sciences, Vol. 21, No. 2, (2021), 29-38

Original Article

Journal homepage: www.bjes.edu.iq
ISSN (Online): 23118385, ISSN (Print): 18146120

Numerical Simulation of Heat Transfer from PV Panel with a Wetted Porous Wick

Angham Fadil Abed [1,*], Dhafeer Manee Hachim [2], Saleh E. Najim [3]

[1] *Department of Mechanical Engineering, College of Engineering, University of Al-Kufa, Najaf, Iraq*
[2] *Engineering Technical College, Al-Furat Al-Awsat Technical University, Najaf, Iraq*
[3] *Department of Mechanical Engineering, College of Engineering, University of Basrah, Basrah, Iraq*
E-mail addresses: angham.alshebly@uokufa.edu.iq , coj.dfr@atu.edu.iq , saleh.najim@uobasrah.edu.iq
Received: 7 April 2021; Accepted: 1 June 2021; Published: 11 July 2021

Abstract

The panel absorbed solar radiation and majority of this radiation is transform into a heat, and it is usually wasted and useless. At higher cell temperature, the current out of the cell has an unnoticeable rise, but the voltage value will drop significantly, resulting in a reduction in maximum power produced. The cooling method is therefore beneficial to keep the panel at the operation temperature. A simulation model is developed using COMSOL Multiphysics software version 3.5 software to investigate the enhancement in performance of a PV water cooling module (PVW module) based on a passive and simple cooling technique using a wetted cotton porous wick attached on the PV panel's back side and compare with uncooled PV panel (PVREF module). Unsteady, laminar and 2-D, the flow in the proposed modules is assumed. The input parameters were taken from a real weather condition was perform in Najaf-Iraq. The effect of variation of mass flow rate is also studied in the present work. Good agreement was obtained for PVREF module with previously researches.

Keywords: Evaporating Cooling, PV, Porous Wick, Numerical Simulation.

http://dx.doi.org/10.33971/bjes.21.2.5

1. Introduction

Renewable energies are commodities that can be reused due to their environmentally sustainable and renewable properties, which can be repeated in natural forms over and over again. Wind and solar energy are two common renewable energy sources [1]. All the renewable energy sources available, solar energy appears to be the most promising and long-term [2]. Photovoltaic (PV) technologies are at the top of the list of solar-powered applications, with global solar photovoltaic power supply estimates predicting that PV technologies will deliver 345 GW and 1081 GW in the next 12 years, respectively [3]. Photovoltaic technology is one of the renewable technologies that can be used to create a potential electricity system that is clean, reliable, scalable, and cost-effective. A solar cell is a device that transforms sunlight into DC electricity using semiconductor materials. As photons from sunlight are absorbed and expelled, semiconductor materials allow electrons to flow, leaving a hole filled with surrounding electrons. The photovoltaic effect by photon absorption is the name given to this phenomenon of electron flow. PV modules are usually made up of several small PV cells encapsulated in a single solid flat unit to protect the sensitive cells and connecting wires from the harsh environment in which they are mounted. The electrical efficiency of PVs decreases as the temperature rises above 25 °C. The solar cells crystalline silicon efficiency reduces of about 0.5 percent with every 1 °C increase in temperature, and this efficiency reduction varies by cell type [4], [5]. The open voltage circuit decreases as the cell temperature rises. The heat emitted by inactive solar irradiance absorption is the primary cause of temperature rises in photovoltaic modules. The most important time in decreasing PV panel efficiency is in regimes with the highest levels of solar irradiation and lowest wind air velocities [6], [7]. As a result, the cooling method is advantageous in maintaining the cell's working temperature. Active cooling and passive cooling are the two most popular PV cooling methods. PV active cooling uses external power to improve heat transfer between the PV and the cold source, while passive cooling needs external energy and additional power consumption [8], [9].

Haidare et al. [10], investigated the impact of evaporative cooling on solar photovoltaic (PV) panels experimentally. The heat generated by the PV module's body was absorbed by the latent heat of evaporation, lowering its temperature. Under outdoor conditions, the experimental setup was designed, assembled, and tested in an efficient and simple manner. PV panel rear surface was wet by the water and exposed to the environment. Gravity was used to deliver water from a tank to the back of the PV panel. A series of experiments were carried out and evaluated in real conditions in Riyadh City, demonstrating the process' efficiency. More than 20 °C reduction in PV panel temperature and about 14 percent increase in electrical power generation were achieved compared to a reference PV panel. Lucas et al. [11], experimentally evaluated PV panel performance electrically and thermally which was cooled by evaporating chimney. Reduction in temperature and electrical efficiency

enhancement were obtained, around 8 °C was reduced, and the average electrical efficiency increase was 4.9 to 7.9 percent. The average ambient temperature is, however, lower than 30 °C. Chandrasekaretal [12], proposed a cooling system with a cotton wick structures in combination with aluminum heat spreader to overcome high temperature during the conditions of higher ambient. Experiments with a 25 Wp PV module were carried out for this study motivation at Tiruchirappalli, India (78.6 E & 10.8 N). A reduction in PV module maximum temperature of about 6 °C is obtained. This leads to a decrease in module temperature of around 12 percent due to the cooling impact used by the fin effect of the heat spreader on the back side and the evaporative cooling. Hasan et al. [13], suggested a new cooling method for cooling PV by using array of a pin fins heat sink as well as moist wood wool pad. The latest cooling system technique is built on the principle of extended surfaces heat transfer (fins) and evaporative cooling. A decrease in the solar panel operating temperature and subsequently improvements in results were obtained. The decrease in the temperature of the module was about 26.05 percent. Results shows the power output and the panel efficiency enhancements was around 32.7 and 31.5 percent, respectively. Slimani et al. [14], proposed a comparative analysis for four solar system devices. The numerical results of the daily average overall efficiency show that 29.63 percent for photovoltaic module (PV-I), 51.02 percent for conventional hybrid solar air collector (PV/T-II), 69.47 percent for glazed hybrid solar air collector (PV/T-III) and 74 percent for glazed double-pass hybrid solar air collector (PV/T-IV). The results accomplished with air flow rate of 0.023 kg/s and with a summary pattern of weather data obtained by experimentation collected at the Algiers location in a sunny day. Haidar et al. [15], perform a theoretical analysis to show the impact of evaporative cooling on the PV performance. The study involves a water layer flowing within a duct, heat and mass transfer between this layer and air is blown within the same duct, in addition a heat transfer from the PV panel to the ambient air. The results obtained demonstrate the influence on the cooling process of certain geometrical parameters such as air flow rate, temperature and humidity. In particular, it was found that the PV panel temperature decreases significantly when the air inlet temperature decreases. A decrease of about 6 °C in PV panel temperature was expected.

The present work is an attempt to investigate numerically the cooling and enhance the performance of PV module by using a simple passive cooling technique based on water cooling by using a wetted cotton porous wick fixed at rear PV surface. The input parameters were taken from a real weather condition was perform in Najaf-Iraq (30° slope PV panel is installed to obtain maximum solar radiation and 32.1 a latitude angle). A cooling system was providing in the back surface of PV panel by employing a wetted cotton porous wick to cool the PV and to increase electrical power. The model equations are continuity, momentum, energy equations and were solving using COMSOL Multiphysics software version 3.5.

2. System description

Figure 1 shows a proposed modules sectional view. Two PV module with a peak power of the same (52 W) are employed in the simulation. One simulation includes PV module without any modifications (PVREF) which is assumed as reference non cooling module and another PV module are supplied with a cooling system (PVW). For PVW module a piece of plain porous cotton wick of 0.01 mm thickness was attached directly to the PV rear surface in order to cool the panel. The wick was wetted by a flowing water from the top and the excessive hot water dropping from bottom. Solar energy raises the panel temperature and the wick layer. Some of flowing water on the wick converted and evaporate to ambient and some of water are extracted out the module from the bottom. It can be seen from Fig. 1 (a), PVREF consist of three layers (front glass layer *fg*, solar cell layer *sc*, back sheet layer b). PVW have the same layers with additional layer for wetted wick in the rear surface of the back sheet layer Fig. 1 (b). Table 1 gives the design simulation parameters and thermo-physical properties that are used. The modules are tilted at an angle of 30° to ensure the solar radiation are normal to the PV surface at most day times.

Table 1 the material, item, symbol, and values of hybrid modules used in the simulation.

Part	Material	Item	Symbol	Value (m)
PV front glass cover	glass	Thickness	t_{fg}	0.0032
		Length	l_{pv}	0.539
		Width	w_{pv}	0.66
PV solar cells	Silicon	Thickness	t_{sc}	0.0003
		Length	l_{pv}	0.539
		Width	w_{pv}	0.66
PV back sheet	Tedler	Thickness	t_b	0.0005
		Length	l_{pv}	0.539
		Width	w_{pv}	0.66
Wick	Cotton	Thickness	t_w	2.1E-4
		Length	l_{pv}	0.539
		Width	w_{pv}	0.66

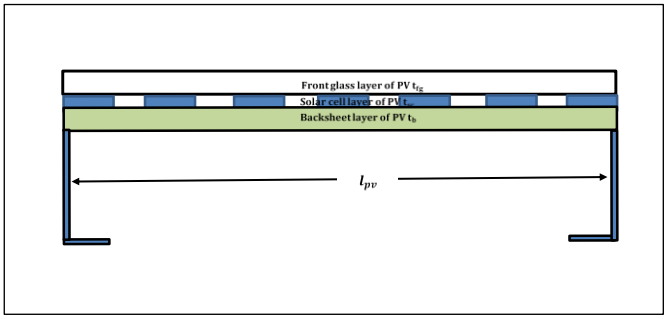

(a)

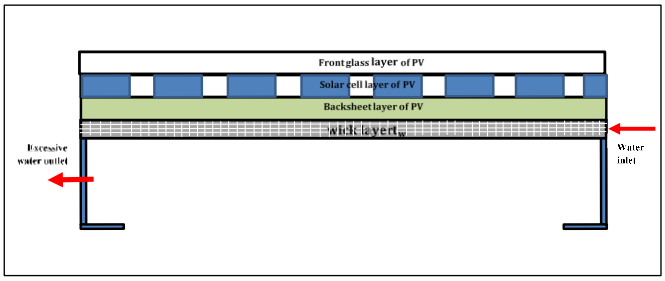

(b)

Fig. 1 Schematic cross-sectional view **(a)** PVREF module **(b)** PVW module.

3. Mathematical simulation

Figure 2 displays the heat transfer modes in the proposed modules. Using time-dependent energy balance, the system equations are modeled and simulated by using a COMSOL software Ver.5.3. The following assumptions are used to express the energy balance equations:

1. Unsteady, laminar and 2-D flow was assumed in the proposed modules.
2. Heat transfer coefficients are dependent on temperature.
3. Lateral sides thermal losses have been ignored.
4. The modules properties are variable (temperature changes).
5. Ground radiation is negligible.

The heat balance equations for each module can be written as:

3.1. PVREF module

3.1.1. Front glass layer

$$M_{fg}\, C_{fg}\, \frac{dT_{fg}}{dt} = R_{fg} - Q_{rfg\text{-}sky} - Q_{cfg\text{-}amb} - Q_{cofg\text{-}sc} \quad (1)$$

Where:

$$R_{fg} = \alpha_{fg}\, I \quad (2)$$

$$Q_{rfg\text{-}sky} = h_{rfg\text{-}sky}\left(T_{fg} - T_{sky}\right) A_m \quad (3)$$

$$Q_{cfg\text{-}amb} = h_{cfg\text{-}amb}\left(T_{fg} - T_{amb}\right) A_m \quad (4)$$

$$Q_{cofg\text{-}sc} = h_{cofg\text{-}sc}\left(T_{fg} - T_{sc}\right) \quad (5)$$

3.1.2. Solar cells layers

$$M_{sc}\, C_{sc}\, \frac{dT_{sc}}{dt} = R_{sc} - Q_{cosc\text{-}fg} - Q_{cosc\text{-}b} - Q_{ele} \quad (6)$$

Where:

$$R_{sc} = \tau_{fg}\, \alpha_{sc}\, I\, \beta \quad (7)$$

$$Q_{cosc\text{-}fg} = h_{cosc\text{-}fg}\left(T_{sc} - T_{fg}\right) A_m \quad (8)$$

$$Q_{cosc\text{-}b} = h_{cosc\text{-}b}\left(T_{sc} - T_b\right) A_m \quad (9)$$

$$Q_{ele} = I\, A_m\, \zeta_{ref}\left[1 - \beta_p\left(T_{sc} - T_{sc,ref}\right)\right] \quad (10)$$

3.1.3. Back sheet layer

$$M_b\, C_b\, \frac{dT_t}{dt} = R_b + Q_{cosc\text{-}b} - Q_{cb\text{-}amb} \quad (11)$$

Where:

$$R_t = \tau_{fg}^2\, \alpha_t\, I\, (1 - \beta) \quad (12)$$

$$Q_{cosc\text{-}b} = h_{cosc\text{-}b}\left(T_{sc} - T_b\right) A_m \quad (13)$$

$$Q_{cb\text{-}amb} = h_{cb\text{-}amb}\left(T_b - T_{amb}\right) A_m \quad (14)$$

3.2. PVW module

The cooling system was attached on the back side of the PV in the current study, all equations balance that was carried out for PVREF module was applied here, the only difference is in back sheet layer equations.

3.2.1. Back Sheet Layer

$$M_b\, C_b\, \frac{dT_b}{dt} = R_b + Q_{cosc\text{-}b} - Q_{cb\text{-}w} \quad (15)$$

Where:

$$Q_{cb\text{-}w} = h_{cb\text{-}w}\left(T_b - T_w\right) A_m \quad (16)$$

R_b and $Q_{cosc\text{-}b}$ from eq. (12 and 13).

3.2.2. Wick Layer

$$M_w\, C_w\, \frac{dT_w}{dt} = Q_{cb\text{-}w} - Q_{cw\text{-}amb} + C_w\, \dot{m}_i\, (T_{iw} - T_{ew}) \quad (17)$$

Where:

$$Q_{cw\text{-}amb} = h_{cw\text{-}amb}\left(T_w - T_{amb}\right) A_m \quad (18)$$

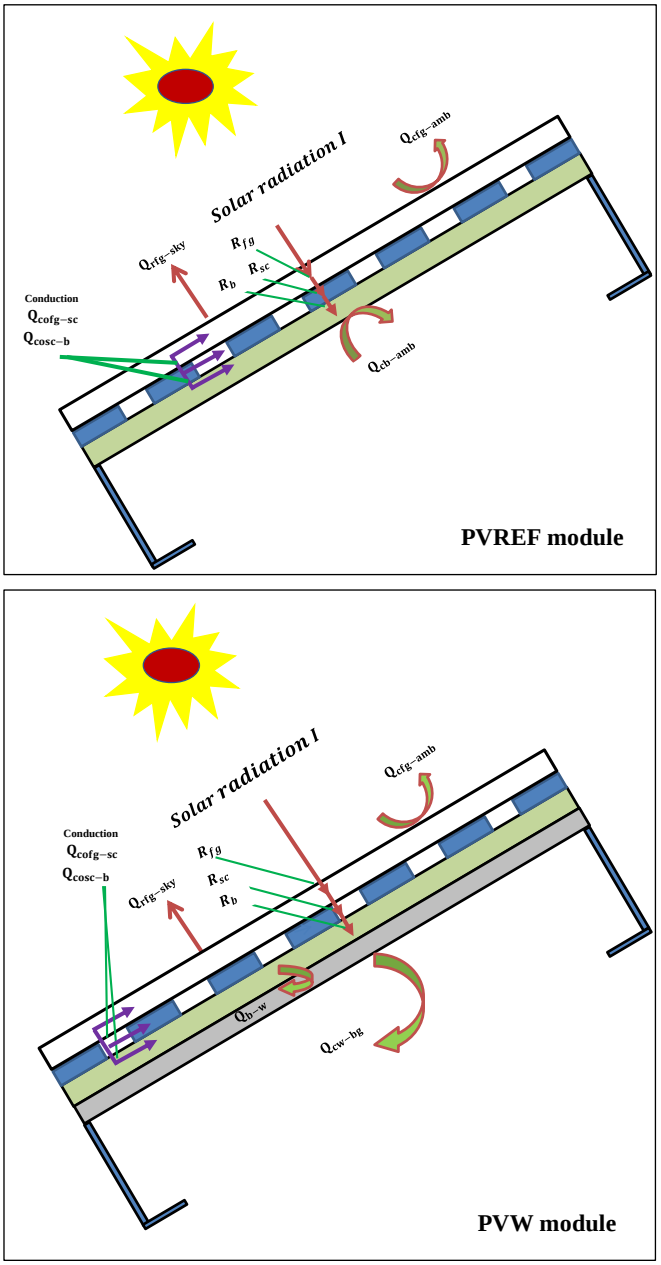

Fig. 2 Types of heat transfer modes for PVREF and PVW modules.

4. Electrical and thermal efficiency

For PVREF and PVW modules the electric efficiency was expressed as [14]:

$$\zeta_{ele} = \frac{Q_{ele}}{I\,A_m} \tag{19}$$

Equation (10) was applied to find Q_{ele}. PVREF does not have any beneficial thermal energy. PVW thermal efficiency was expressed as [16]:

$$\zeta_{th} = \frac{C_w\,\dot{m}_i\,(T_{iw} - T_{ew})}{I\,A_m} \tag{20}$$

5. Coefficients of heat transfer

5.1. Coefficient of radiation heat Transfer

Radiation heat transfer from the PV front glass cover to the sky was written as

$$h_{rfg\text{-}sky} = \sigma\,\varepsilon_{fg}\,\frac{(T_{fg}^2 - T_{sky}^2)(T_{fg}^2 + T_{sky}^2)}{T_{fg} - T_{sky}} \tag{21}$$

Where:

$$T_{sky} = 0.0552\,T_a^{1.5} \tag{22}$$

5.2. Coefficient of convection heat transfer

Convection heat transfer coefficient from external layers to ambient produce from effect of wind and can be express for all modules as [14]:

$$h_{cj\text{-}amb} = 5.7 + 3.8\,V_w \tag{23}$$

5.3. Coefficient of conduction heat transfer

The conduction heat transfer is between two adjacent module layers and can be written between layers j and m as [14]:

$$h_{coj\text{-}m} = 1\Big/\left(\frac{l_j}{k_j} + \frac{l_m}{k_m}\right) \tag{24}$$

6. Governing equations

The governing equations are simulated on the principles of conservation of continuity, momentum and energy. Process of heat transfer start when the solar radiation is falling on the panel. In the present modules, fluid flow was assumed incompressible, laminar, unsteady, and 2D. The following governing equations were applied:

6.1.1. Conservation of continuity equation

For porous wick layer the continuity equation can be written as [17]:

$$\rho\nabla.(u) = Q_{br} \tag{25}$$

6.1.2. Conservation of momentum equation

The equation of momentum for porous layer is:

$$\rho\frac{1}{\epsilon_p}\left(\frac{\partial u}{\partial t} + \frac{1}{\epsilon_p}\,u.\nabla u\right) = -\nabla p\,I + \nabla.\left(\mu\frac{1}{\epsilon_p}(\nabla u + (\nabla u)^T)\right) - \left(\mu\kappa^{-1} + \frac{Q_{br}}{\epsilon_p^2}\right)u + (\rho - \rho_{ref})\,g \tag{26}$$

Where $\boldsymbol{u}$ is the fluid velocity, $\boldsymbol{p}$ is the fluid pressure, $\boldsymbol{\rho}$ is the fluid density, $\boldsymbol{\mu}$ is the fluid dynamic viscosity, $\boldsymbol{\kappa}$ is permeability and $\boldsymbol{\epsilon_p}$ is porosity. Where viscous losses in the porous layer are represented by the third term on the right-hand side. A combination of the continuity equation (25) and the momentum equation (26), which together form the Brinkman equations, governs the flow in porous media.

6.1.3. Conservation of energy equation

The energy equation can be expressed as:

$$\rho\,C\,\frac{\partial T}{\partial t} + \rho\,Cu\,\nabla T + \nabla q = q_o \tag{27}$$

Where:

$$q = -\,K\,\nabla T \tag{28}$$

and q_o represent heat source

For porous layer the equation becomes:

$$(\rho\,C)_{eff}\,\frac{\partial T}{\partial t} + \rho\,Cu\,\nabla T + \nabla q = q_o \tag{29}$$

Where:

$$q = -\,K_{eff}\,\nabla T \tag{30}$$

The effective thermal conductivity and heat capacity can be found as:

$$(\rho\,C)_{eff} = \theta_p\,\rho_p\,C_p + (1 - \theta_p)\,\rho\,C \tag{31}$$

$$K_{eff} = \theta_p\,K_p + (1 - \theta_p)\,K \tag{32}$$

Where volume fraction is

$$\theta_p = 1 - \epsilon_p \tag{33}$$

6.2. Boundary conditions

To model the equations of continuity, momentum, and energy, suitable boundary conditions must be chosen at all boundaries and defined. PVREF boundary conditions can be expressed as:

1. For front glass layer, convection to ambient,

$$h_{cfg\text{-}amb} = 5.7 + 3.8\,V_w \tag{34}$$

Radiation to ambient,

$$h_{rfg\text{-}sky} = \sigma\,\varepsilon_{fg}\,(T_{fg}^4 - T_{sky}^4) \tag{35}$$

Heat source, $Q = R_{fg}$

2. For solar cell, Heat source

$$-\,n.Q = (R_{sc} - Q_{ele}) \tag{36}$$

3. For back sheet layer, convection to ambient,

$$h_{cb\text{-}amb} = 5.7 + 3.8\,V_w \tag{37}$$

Heat source, $Q = R_{sc}$

4. The same boundary conditions for PVREF can be applied here for PVW except for back sheet and wick layers which can be written as:
Wick surface: At inlet $\dot{m} = \dot{m}_i$, $T = T_{iw}$, at outlet $p = 0$, along the surface of wick, $T = T_w$, $-n.Q = -Q_{cw\text{-}amb}$
Side walls: No-slip, thermal insulation and no flux.

6.3. Initial conditions

The initial conditions for the governing equations that was displayed in section 6 represent a start of simulation at $t = 0$ and can be written as follow:

1. Continuity and momentum equation: The initial value of the velocity field is zero;
   $u\,(x, y, t = 0) = v\,(x, y, t = 0) = 0$
2. Energy equation: $T\,(x, y, t = 0) = T_{amb}$ (t = 9:00 AM)

6.4. Meshing and grid dependence test

To verify the mesh size for the models, a grid dependency test was performed. The meshing adopting finite element for the present modules (PVREF, PVW) computational domain is performed and one of these modules (PVW) was shown in Fig. 3. The subdomain and boundary elements have been chosen as free triangular forms in the present numerical model. Various forms of non-uniform systems grid were tested with elements for PVW: 24689, 24966, 26660, 27770 and PVREFF: 19382, 22681, 21072, 28033, 28064. Supervisory parameters are selected such as back sheet temperature and was evaluated in order to study the independency of grid. It was observed that there is no considerable difference in the back sheet temperature value for normal and fine type meshing for PVW and PVREF respectively, but in more time is needed for simulation in COMSOL. Thus, for the numerical analysis to save time, the PVW and PVREFF models with 27770 and 28064 domain elements are chosen to be no change in the result when increasing the elements number over the value select. The outcome of the grid study testing is display in the Table 2.

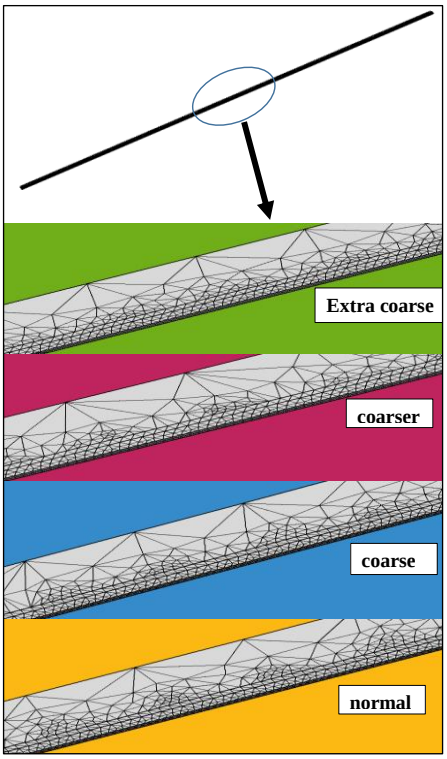

Fig. 3 Different types of meshing for PVW module.

Table 2 Grid sensitivity check for PVREF and PVW.

Type of meshing	Extra coarse	coarser	coarse	normal	fine
Elements (PVW)	24689	24966	26660	27770	
T_b	70.436	70.921	70.619	70.213	
Elements (PVREF)	19382	22681	21072	28033	28064
T_b	74.634	74.502	74.179	74.593	74.593

6.5. Validation

The validity of the current 2D simulation was established for PVREF. The findings of the numerical simulation found by [14] were compared to the results of the current PVREF model. For this validation setup the weather conditions from the experimental work [18] and the design parameters explained in Table 3 are chosen to compare and evaluate the energy performance for the PVREF module in this simulation study. To compare the results obtained by this study's numerical model with those obtained by [14], the percent of root mean square deviation (RMSD) was used as follows:

$$RMSD\ (\%) = 100 \times \sqrt{\frac{\sum_1^n \left(\frac{X_{sim,i} - X_{exp,i}}{X_{sim,i}}\right)^2}{n}} \tag{38}$$

where $X_{sim,i}$, $X_{exp,i}$, $\boldsymbol{i}$ and $\boldsymbol{n}$ are respectively, the value from simulation, the value from experimental, and the number of data. The value RMSD equal to zero in ideal case. Fig. 4 displays the graphical diagram of the simulated PVREF solar cell and back sheet temperature values and their corresponding Silimin et al. [14] expected values during the day of the test. Between the simulated results, a good agreement is found.

Table 3 the design parameters of modules used during the validation setup [14].

Parameters	Value
The length of the PV module, l_{pv}	1.28 m
The width of the PV module, W_{pv}	0.32 m
The module area, A_m	1.28 × 0.32 m^2
The thickness of front glass cover, t_{fg}	0.0032 m
The heat conductivity of front glass cover, K_{fg}	1 W/m K
The absorptivity of glass cover, α_{fg}	0.06
The transmissivity of glass cover, τ_{fg}	0.84
The emissivity of glass cover, ε_{fg}	0.93
The thickness of solar cell, t_{sc}	0.0003 m
The absorptivity of solar cell, α_{sc}	0.85
The heat conductivity of solar cell, K_{sc}	0.036 W/m K
The thickness of back sheet, t_b	0.0005 m
The heat conductivity of back sheet, K_b	0.033 W/m K
The absorptivity of back sheet, α_b	0.8
The packing factor, β	0.88
The temperature coefficient, β_p	0.0045
The thermal power conversion factor, Cf	0.36

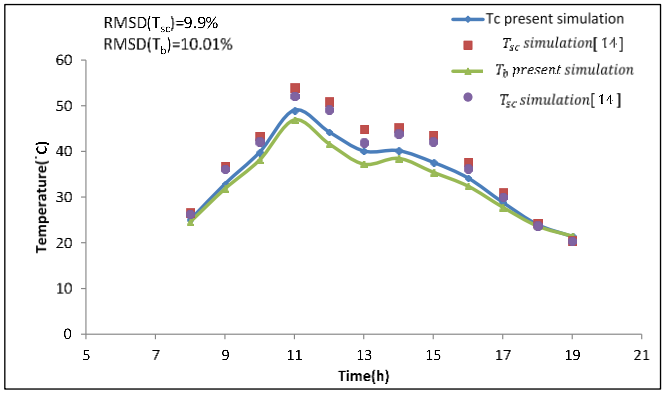

Fig. 4 the simulated results of solar cells and back sheet temperatures during the test day for PVREF.

7. Results and discussion

To solve the governing equations to predicate the measured parameters the COMSOL Multiphysics ver. 5.0 programs are used. The input parameter which includes (solar radiation, ambient temperature, wind speed, water inlet temperature) used in COMSOL software are taken from experimental data for clear sunny day on (9 September 2019) in Najaf-Iraq for all simulated results which studied the effect of flow patterns, temperature distribution, mass flow rate, … etc. The numerical results are presented for PVREF and PVW modules.

7.1. Weather conditions

Figure 5 presented the hourly variation of average solar radiation and temperature of ambient for testing day (9 September 2019). The readings of the experiments are taken on an hourly basis from 9:00 AM to 16:00 PM. The radiation intensity at noon is as high as 1021 W/m^2. It can be seen that the average temperature of ambient change between 40.3 °C to a higher value of 49.8 °C in this day. The variation of wind speed with time was displayed in Fig. 6. The average of wind speed during the testing day was around 0.262 m/s.

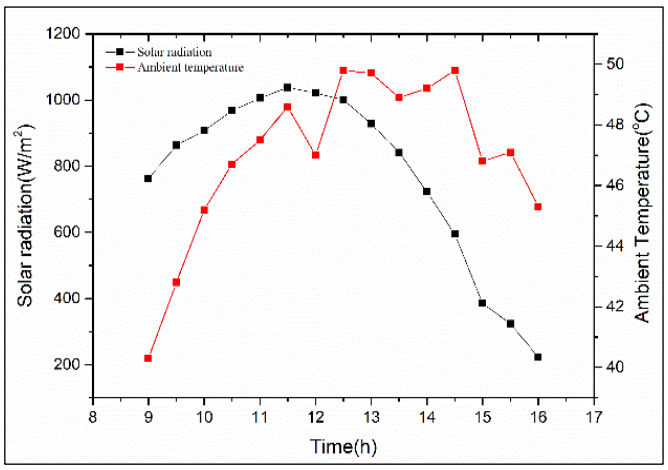

Fig. 5 Hourly variation of radiance and ambient temperature during the test day.

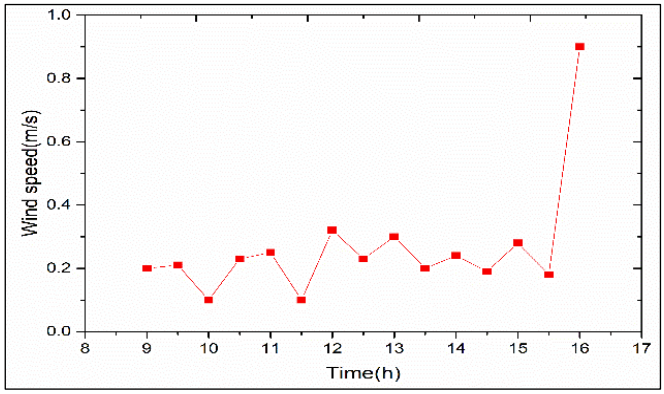

Fig. 6 Hourly variation of wind speed during the test day.

7.2. Flow Patterns and temperature distribution

Figure 7 (a) shows the flow pattern inside the wick layer at highest solar radiation (12:00 PM). It can be seen the development of boundary layer and the no slip condition at the walls. The red color shows higher velocity of water while blue color showing zero velocity. Figure 7 (b) indicate the temperature distribution for PVW and PVREF modules. PVREF shows higher temperature than PVW. The gradient in temperature for PVW is very clear and wick layer shows the lower temperature than other PVW components.

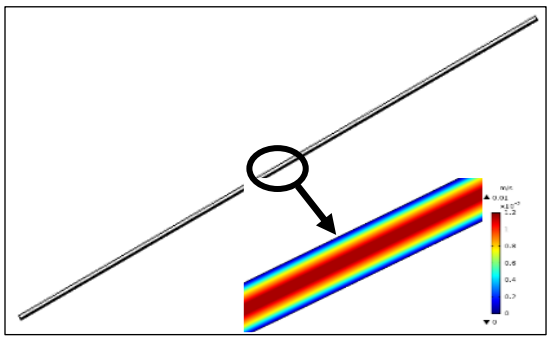

(a)

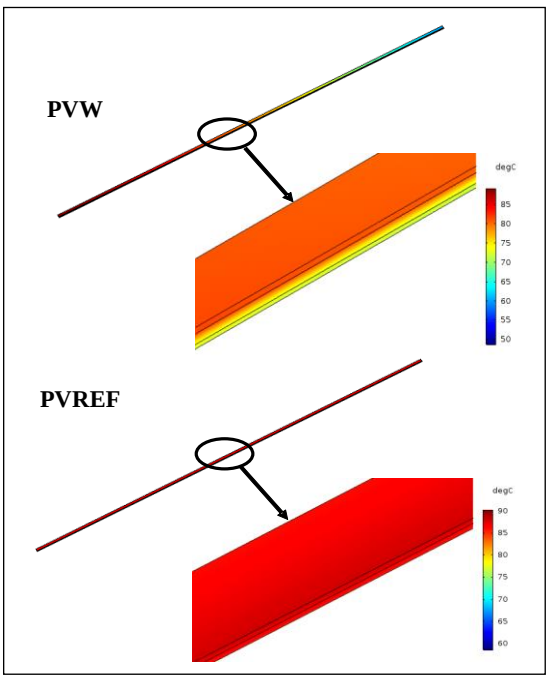

Fig. 7 (a) Flow pattern through a wick layer for PVW Module. **(b)** Temperature distribution for PVW and PVREF modules.

7.3. Average temperature distribution

The influence of water cooling on the temperature of PV module (front and back surface) during the day is indicated in Figs. 8 and 9. It can be seen the temperatures of PVREF module is higher than PVW module. The variation of average back sheet temperature for the module cooling (PVW) and for the non-cooling module (PVREF) is displayed and respective average maximum back sheet temperatures for PVREF module was about 86.79 °C which was reduced to about 78.48 °C in PVW module Fig. 8. Cooling the module causes reduction in temperature of about 9.57 %. This reduction in temperature produce enhancement in electrical efficiency. The maximum front glass temperature for cooling (PVW) and non-cooling (PVREF) cases was 85.17 °C and 87.73 °C respectively Fig. 9. Therefore, PVW front glass temperature shows a 2.91 % percentage reduction. This percentage is reasonable as compared with the low mass flow rate of cooling fluid that was used in the simulation. Figure 10 present the hourly variation of average wick and inlet water temperatures. Wick shows higher temperature than inlet water temperature which indicate the effectiveness of using porous wick in the back surface of the panel to reduce high panel temperature.

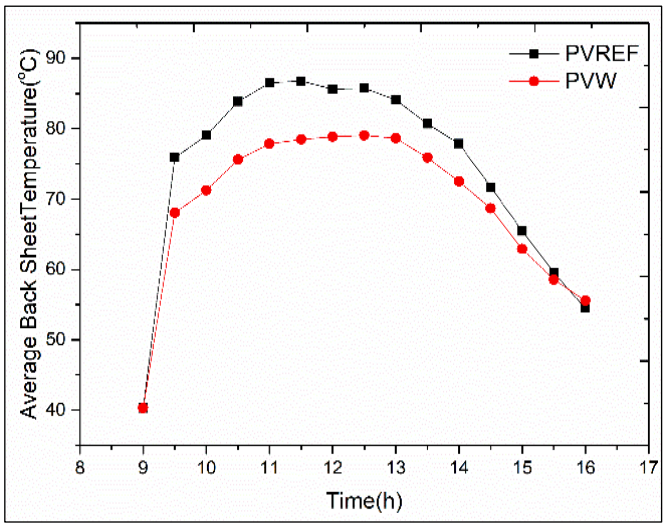

Fig. 8 Hourly variation of average back sheet temperatures for PVW and PVREF during the test day.

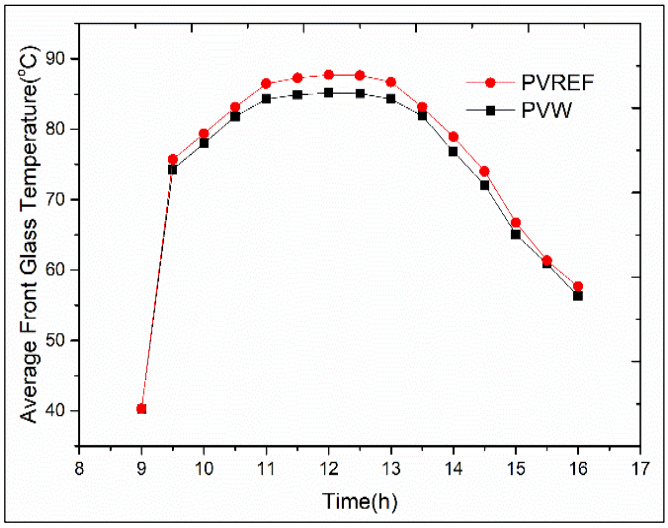

Fig. 9 Hourly variation of average front glass temperatures for PVW and PVREF during the test day.

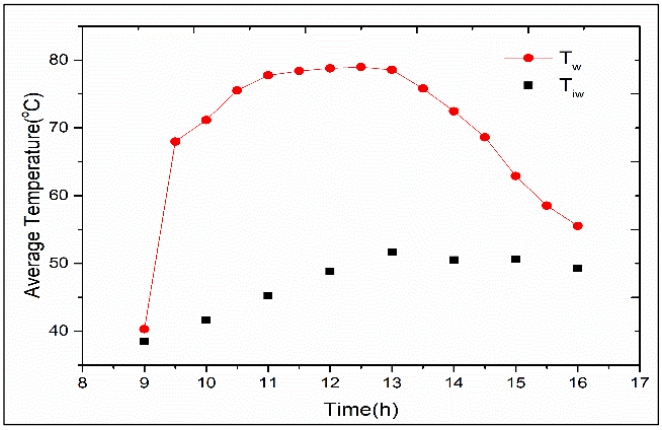

Fig.10 Hourly variation of average wick and inlet water temperatures for PVW during the test day.

7.4. Effect of mass flow rate

The mass flow rates used in simulation was taken from several our experiments that was carried in order to prevent excessive water to dropping from the wick. Figure 11 (a) and (b) indicate the effect of variation mass flow rates (5.55E-4 kg/s, 8.333E-4 kg/s, 0.0011 kg/s) with time on average back sheet and front glass temperatures. It was seen that the back sheet and front glass temperatures is high when the flow rate is low but the temperatures reduces when the flow rate is high. This is because the velocity of the fluid increases when the mass flow increases, resulting an increase in convective heat transfer from back sheet layer to the wick layer.

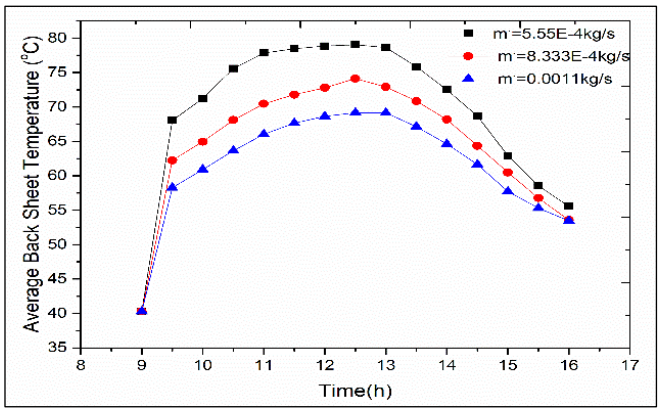

(a)

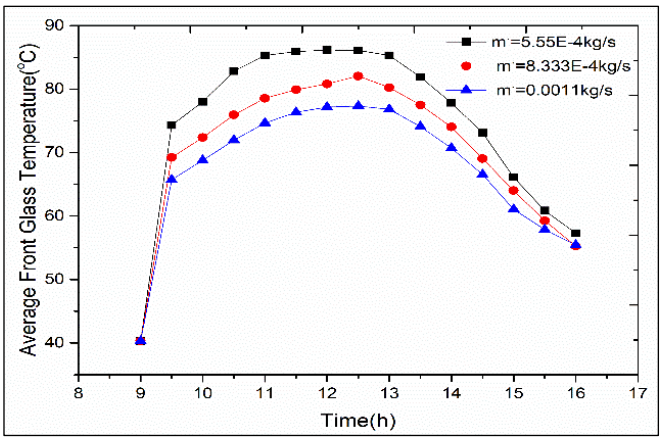

Fig. 11 variation of **(a)** average back sheet temperature and **(b)** average front glass temperature for PVW during the test day at different mass flow rate.

7.5. Electrical and thermal efficiencies

The electric power hourly variations produced form PVW and PVREF modules are shown in Fig. 12. PVREF module shows the lowest electrical power. The maximum electrical output power of non-cooling module (PVREF) was 36.47 W at 12:00 AM while the maximum output power of cooling module (PVW) was 40.79 W. The enhancement in electrical power output of PVW module was 10.59 %. Figure 13 shows the hourly variations of the thermal efficiency for the PVW module. It can be seen the thermal efficiency is low at morning because low solar radiation and a little difference between inlet and outlet water temperature and starting to increase. The maximum thermal efficiency was obtained about 38.92 %. The variation of electrical efficiency with time for tow modules was displayed in Fig. 14. PVW shows higher electrical efficiency than PVREF because of good cooling method that was used. The maximum electrical efficiency for PVW and PVREF was 11.25 % and 10.06 % respectively. The overall efficiency hourly variations of each module are displayed in Fig. 15. The maximum overall efficiency for PVW and PVREF are 69.7 % and 34.28 %.

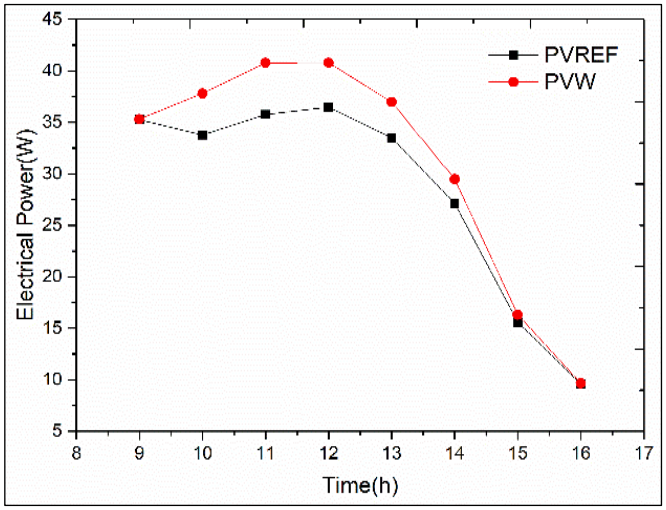

Fig. 12 Hourly variation of electrical power for PVW and PVREF modules.

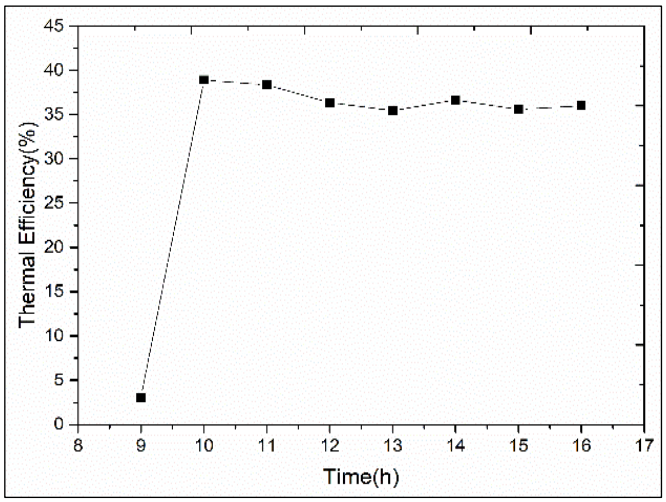

Fig. 13 Hourly variation of thermal efficiency for PVW module.

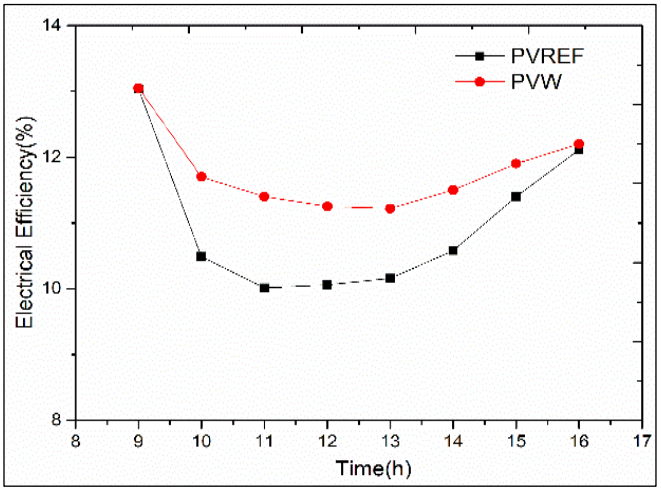

Fig. 14 Hourly variation of electrical efficiency for PVW and PVREF modules.

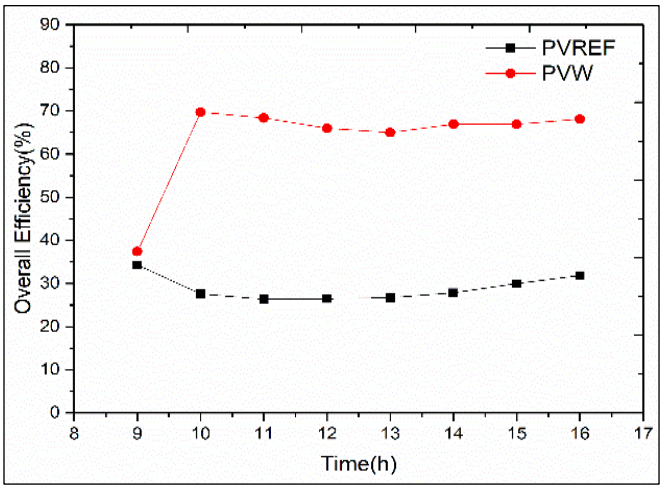

Fig. 15 Hourly variation of overall efficiency for PVW and PVREF modules.

8. Conclusions

Numerical simulation for a passive simple cooling module by using a porous wick made from cotton attached in the back surface of photovoltaic panel was develop to reduce the temperature of module and increase the output power. The suggested module was compared to another uncooled module in terms of electrical and thermal efficiency. The input parameter was derived from Najaf, Iraq's climatic conditions. The following conclusions can be made based on the findings:

1. The maximum back sheet PVREF temperature is reduced from 86.79 °C to 78.48 °C for PVW. This corresponding to a reduction of about 9.57 % in PVW module back sheet temperature. This reduction attributed to the suggested water cooling which employ a wetted porous wick at the rear side of the PV module.
2. The temperature of PV panel increased with an increase in solar radiation.
3. The electrical power for PVW module was enhanced by about 10.59 % due to water cooling at the rear side of the PV module.
4. The influence of mass flow rate on PV temperature, that the back sheet and front glass temperatures is high when the flow rate is low but the temperatures reduces when the flow rate is high.

References

[1] P. K. Halder, N. Paul, M. U. H. Joardder and M. Sarker, "Energy scarcity and potential of renewable energy in Bangladesh", Renewable and Sustainable Energy Reviews, Vol. 51, pp. 1636-1649, 2015.

[2] A. A. K. Ali, "Investigation the Performance of Hybrid Photovoltaic/Thermal Solar System Using Nano-fluid", M.Sc. Thesis, Dep. of Mech. Eng., University of Kerbala, 2019.

[3] A. A. F. Husain, W. Z. W. Hasan, S. Shafie, M. N. Hamidon, and S. S. Pandey, "A review of transparent solar photovoltaic technologies", Renewable and Sustainable Energy Reviews, Vol. 94, pp. 779-791, 2018.

[4] M. Chandrasekar, S. Rajkumar, and D. Valavan, "A review on the thermal regulation techniques for non-integrated flat PV modules mounted on building top", Energy Build, Vol. 86, pp. 692-697, 2015.

[5] H. A. Ali Al-Waelia, K. Sopiana, A. Hussein Kazemb, and T. Miqdam Chaichanc, "Photovoltaic/Thermal (PV/T) systems: Status and future prospects", Renewable and Sustainable Energy Reviews, Vol. 77, pp. 109-130, 2017.

[6] A. A. B. Baloch, H. M. S. Bahaidarah, P. Gandhidasan, and F. A. Al-Sulaiman, "Experimental and numerical performance analysis of a converging channel heat exchanger for PV cooling", Energy Conversion and Management, Vol. 103, pp. 14-27, 2015.

[7] A. S. Abdelrazik, F. Al-Sulaiman, R. Saidur, and R. Ben-Mansour, "A review on recent development for the design and packaging of hybrid photovoltaic/thermal (PV/T) solar systems", Renewable and Sustainable Energy Reviews, Vol. 95, pp. 110-129, 2018.

[8] A. M. Elbreki, M. A. Alghoul, K. Sopian and T. Hussein, "Towards adopting passive heat dissipation approaches for temperature regulation of PV module as a sustainable solution", Vol. 69, pp. 961-1017, 2017.

[9] S. Jamali, M. Yari and S. M. S. Mahmoudi, "Enhanced power generation through cooling a semi-transparent PV power plant with a solar chimney", Energy Conversion and Management, Vol. 175, pp. 227-235, 2018.

[10] Z. A. Haidar, J. Orfi, and Z. Kaneesamkandi, "Experimental Investigation of Evaporative Cooling for Enhancing Photovoltaic Panels Efficiency", Results in Physics, Vol. 11, pp. 690-697, 2018.

[11] M. Lucas, F. Aguilar, J. Ruiz, C. Cutillas, A. Kaiser, and P. Vicente, "Photovoltaic Evaporative Chimney as a new alternative to enhance solar cooling", Renewable energy, Vol. 111, pp. 26-37, 2017.

[12] M. Chandrasekar and T. Senthilkumar, "Experimental demonstration of enhanced solar energy utilization in flat PV (photovoltaic) modules cooled by heat spreaders in conjunction with cotton wick structures", Energy, Vol. 90, Part 2, pp. 1401-1410, 2015.

[13] I. A. Hasan, I. S. kareem and D. A. Attar, "Effect of Evaporative Cooling Combined with Heat Sink on PV Module Performance", Journal of University of Babylon for Engineering Sciences, Vol. 27, No. 2, pp. 252-264, 2019.

[14] M. E. Slimani, M. Amirat, I. Kurucz, S. Bahria, A. Hamidat and W. B. Chaouch, "A detailed thermal-electrical model of three photovoltaic/thermal (PV/T) hybrid air collectors and photovoltaic (PV) module: Comparative study under Algiers climatic conditions", Energy Conversion and Management, Vol. 133, pp. 458-476, 2017.

[15] Z. A. Haidar, J. Orfi, H. F. Oztop and Z. Kaneesamkandi, "Cooling of Solar PV Panels using Evaporative Cooling", Journal of Thermal Engineering, Vol. 2, No. 5, pp. 928-933, 2016.

[16] S. H. Aybar, "Mathematical modeling of an inclined solar water distillation system", Desalination, Vol. 190, Issus 1-3, pp. 63-70, 2006.

[17] R. Rieck, A. Benard and C. Petty, "Reynolds Number Dependent Porous Media Flow Using the Brinkman Equation", Excerpt from the Proceedings of the COMSOL Conference, Boston, 2009.

[18] A. S. Joshi, A. Tiwari, G. N. Tiwari, I. Dincer and B. V. Reddy, "Performance evaluation of a hybrid photovoltaic thermal (PV/T) (glass-to-glass) system", International Journal of Thermal Sciences, Vol. 48, Issue 1, pp.154-164, 2009.

Nomenclature

Symbol	Definition	Unit (SI)
A_m	Area of panel	m^2
C_i	Specific heat capacity of a component i	J/kg. K
C_f	Conversion factor of thermal power plant	
g	Gravitational acceleration (9.807)	m/s^2
h_c	Convection heat transfer coefficient	W/m^2. K
$h_{coi\text{-}j}$	Conduction heat transfer coefficient through adjacent components	W/m^2. K
h_r	Radiation heat transfer coefficient	W/m^2. K
I	Intensity of solar radiation	W/m^2
K	Thermal conductivity	W/m.K
l_{pv}	length of PV panel	m
M_i	Mass of a component i	kg
$\dot{m}$	Mass flow rate	kg/s
p	Fluid pressure	Pa
Q	Heat source	W
Q_{br}	Mass source	$kg/(m^3.s)$
Q_c	Convective heat transfer	W
Q_{co}	Conductive heat transfer	W
Q_{ele}	Electric power useful	W
Q_r	Radiative heat transfer	W
q	Heat flux by conduction	W/m^3
q_o	Heat source	W/m^3
R_b	Solar energy absorbed by the back sheet layer of the panel	W
R_{fg}	Solar energy absorbed by front glass layer of the panel	W
R_{sc}	Solar energy absorbed by solar cells layer of the panel	W
T	Temperature	°C
t	Time, Thickness of a component i	m
u	Velocity vector, fluid velocity	m/s
v_w	Wind velocity	m/s
w_{pv}	Width of PV panel	
x, y	Axes	m

Greek letters		
η	Efficiency	-
τ	Transmissivity	-
ρ	Density	Kg/m^3
α	Absorptivity	-
ε	Emissivity	-
σ	Stefan-Boltzmann constant (5.67×10^{-8})	$W/m^2. K^4$
β	Packing factor	-
β_p	Temperature coefficient	1/K
ν	Kinematic viscosity	m^2/s
μ	Fluid dynamic viscosity	$N.s/m^2$
ϵ_p	Porosity	
κ	Permeability	
θ_p	Volume fraction	

Subscripts	
Symbols	**Definition**
amb	Ambient
b	Back sheet layer of PV panel
fg	Front glass layer of PV panel
eff	Effective
ele	Electrical
j,m	Components of PV module
i	Inlet
w	Wick
th	Thermal
o	Overall
p	Porous media
ref	Reference conditions
sc	Solar cell layer of PV panel
sc,ref	Solar cell at reference conditions
sky	Sky
fg-amb	From front glass to ambient
fg-sc	From front glass to solar cell
sc-b	From solar cell to back sheet
b-w	From back sheet to wick
w-amb	From wick to ambient
iw	Inlet to wick
ew	Outlet from wick

Super subscripts	
T	Transpose matrix

Abbreviations	
Symbol	**Description**
PV	Photovoltaic
RMSD	Root mean square percent deviation
PVW	PV with wick
PVREF	Reference PV